

Powerful t-SNE technique leading to clear separation of type-2 AGN and HII galaxies in BPT diagrams

XUEGUANG ZHANG,¹ YANQIU FENG,¹ HUAN CHEN,¹ AND QIRONG YUAN¹

¹*School of Physics and technology, Nanjing Normal University, No. 1, Wenyuan Road, Nanjing, 210023, P. R. China*

Submitted to ApJ

ABSTRACT

Narrow emission-line galaxies can be distinguished in the well-known BPT diagrams through narrow emission line properties. However, there are no boundaries visible to the naked eye between type-2 AGN and HII galaxies in BPT diagrams, besides the extreme dividing lines expected by theoretical photoionization models. Here, based on powerful t-SNE technique applied to the local narrow emission-line galaxies in SDSS DR15, type-2 AGN and HII galaxies can be clearly separated in the t-SNE determined two-dimensional projected map, and then the dividing lines can be mathematically determined in BPT diagrams, leading to charming harmonization of the theoretical expectations and the actual results from real observed properties. The results not only provide an interesting and robust method to determine the dividing lines in BPT diagrams through the powerful t-SNE technique, but also lead to further confirmation on previously defined composite galaxies more efficiently classified in the BPT diagram of [OIII]/H β versus [NII]/H α .

Keywords: Galaxies:Emission line galaxies – Galaxies:Galaxies nuclei – Galaxies:AGN host galaxies

1. INTRODUCTION

BPT diagrams, named after Baldwin, Phillips, & Terlevich (1981) and the pioneer work on detailed study on classifications of narrow emission-line galaxies in Veilleux & Osterbrock (1987), are firstly proposed in 1980s to show different physical properties of optical narrow emission lines of tens to hundreds of extragalactic emission lines objects. Until now, there are millions of narrow emission-line galaxies. And based on different kinds of central activities, narrow emission-line galaxies can be well classified into two main kinds, type-2 AGN (Active Galactic Nuclei) (narrow emission-line AGN) with central AGN activities and HII galaxies without central AGN activities. Although Type-2 AGN and HII galaxies have similar optical spectral features, properties of optical narrow emission lines can be commonly applied to determine classifications of type-2 AGN and HII galaxies, such as the well-known results in ongoing improved BPT diagrams (Cid Fernandes et al. 2011; Juneau et al. 2014; Kashino et al. 2017; Kewley et al. 2019).

The BPT diagrams well allow the division of narrow emission-line objects in two main branches: one containing HII galaxies and the other containing type-2 AGN (Seyfert galaxies and Low Ionization Nuclear Emission-Line Regions (LINERs)). Not similar as Seyfert galaxies totally powered by central AGN activities, different mechanisms have been applied to LINERs, such as AGN activities (Ferland & Netzer 1983; Halpern & Steiner 1983), shock heating (Heckman 1980; Dopita & Sutherland 1995, 1996), photoionization by young stars (Terlevich & Melnick 1985; Filippenko & Terlevich 1992), photoionization by post-asymptotic giant branch (post-AGB) stars (Binette et al. 1994; Eracleous et al. 2010; Cid Fernandes et al. 2011), etc. More recent review on LINERs in Marquez et al. (2017) have shown that 60% to 90% of LINERs could be well considered as genuine AGN. Therefore, in spite of controversial mechanisms, LINERs have been accepted as a subsample of type-2 AGN in the manuscript.

In the well-known BPT diagrams, between type-2 AGN and HII galaxies, there are no clear dividing boundaries visible to the naked eye. The reported dividing lines by flux ratios of optical narrow emission lines in the BPT diagrams are estimated and determined by expected properties of extreme starbursts and/or AGNs by theoretical photoionization models, such as the results well discussed in Kauffmann et al. (2003); Groves et al. (2004); Kewley et al. (2006); Stasinska et al. (2006); Levesque et al. (2010); Melendez et al. (2014), etc. More recently, de Souza et al. (2017) have studied emission-line galaxy classifications through

probabilistic Gaussian mixture model applied to spectroscopic properties from the SDSS DR7 (Sloan Digital Sky Survey, Data Release 7) and SEAGal/STARLIGHT datasets, and shown the Gaussian components relative to AGN and starforming galaxies. However, the results discussed in [de Souza et al. \(2017\)](#) can not yet lead to apparent dividing lines. Thereby, it is a great pity on loss of determining the dividing lines from properties of observed narrow emission lines of real narrow emission-line galaxies. Here, based on the more recent powerful t-SNE (t-distributed Stochastic Neighbor Embedding) technique ([van der Maaten & Hinton 2008](#); [van der Maaten 2014](#); [Arora, Hu, & Kothari 2018](#)) which have been recently applied in Astrophysics ([Traven et al. 2017](#); [Anders et al. 2018](#); [Steinhardt et al. 2020](#)), we will show actual results on the dividing lines in BPT diagrams from real observed properties of narrow emission lines of local narrow emission-line galaxies, to check whether there are harmonization of theoretical expectations and actual results on the dividing lines between HII galaxies and type-2 AGN in the BPT diagrams. Then, our main results and necessary discussions are shown in Section 2, and conclusions are given in Section 3.

2. MAIN RESULTS AND DISCUSSIONS

Based on properties of optical narrow emission lines of main galaxies, the SQL query (<http://skyserver.sdss.org/dr15/en/tools/search/sql.aspx>) can be conveniently applied in SDSS DR15 ([Aguado et al. 2019](#); [Belfiore et al. 2019](#)), leading to collected 35857 local narrow emission line objects with apparent narrow emission lines (line intensities at least 5 times larger than their corresponding measured errors) of $H\alpha$, $H\beta$, $[O III]\lambda 5007\text{\AA}$, $[O I]\lambda 6300\text{\AA}$, $[N II]\lambda 6583\text{\AA}$ and $[S II]\lambda 6717, 6731\text{\AA}$ but no broad emission lines in high-quality SDSS spectra (signal-to-noise ratios larger than 10). The applied SQL query in detail is as follows,

```
SELECT plate , fiberid , mjd , z , snmedian , h_beta_flux , h_beta_flux_err , h_alpha_flux ,
      h_alpha_flux_err , oiii_5007_flux , oiii_5007_flux_err , nii_6584_flux ,
      nii_6584_flux_err , sii_6717_flux , sii_6717_flux_err , sii_6731_flux ,
      sii_6731_flux_err , oi_6300_flux , oi_6300_flux_err
FROM GalSpecLine as G JOIN SpecObjall as S ON S.specobjid = G.specobjid
WHERE S.class = 'GALAXY' and S.SNmedian > 10 and S.z < 0.2 and S.zwarning = 0
      and G.h_beta_flux_err > 0 and G.h_beta_flux > 5*G.h_beta_flux_err and
      G.h_alpha_flux_err > 0 and G.h_alpha_flux > 5*G.h_alpha_flux_err and
      G.oiii_5007_flux_err > 0 and G.oiii_5007_flux > 5* G.oiii_5007_flux_err and
      G.nii_6584_flux_err > 0 and G.nii_6584_flux > 5*G.nii_6584_flux_err and
      G.oi_6300_flux_err > 0 and G.oi_6300_flux > 5* G.oi_6300_flux_err and
      G.sii_6717_flux_err > 0 and G.sii_6717_flux > 5* G.sii_6717_flux_err and
      G.sii_6731_flux_err > 0 and G.sii_6731_flux > 5* G.sii_6731_flux_err and
      (S.subclass = 'STARFORMING' or S.subclass = 'STARBURST' or S.subclass = 'AGN')
      and G.h_alpha_flux/G.h_beta_flux < 6 and G.h_alpha_flux/G.h_beta_flux > 2
      and veldisp > 60 and veldisp < 400 and veldisperr > 0 and veldisp > 5*veldisperr
```

Then, based on the collected properties of narrow emission lines of the 35857 local narrow emission-line galaxies, beautiful BPT diagrams are shown in top panels in Figure 1, It is clear there are no apparent boundaries visible to the naked eye between the expected type-2 AGN locating in top-right regions and the expected HII galaxies locating in bottom-left regions in the shown BPT diagrams. Therefore, it is a constructive challenge to determine the dividing lines through mathematical visualization techniques applied to the real observed narrow emission-line galaxies, besides the theoretical model determined ones.

The two well-known mathematical techniques have been accepted to do visualization and reduction of high dimensional data, the commonly known PCA (Principal Component Analysis) technique ([Ian Jolliffe & Cadima 2016](#); [Lever, Krzywinski, & Altman 2017](#)) and the more recent powerful t-SNE technique ([van der Maaten & Hinton 2008](#); [van der Maaten 2014](#); [Arora, Hu, & Kothari 2018](#)). The PCA technique has been well applied in Astronomy for several decades, such as the results reported in [Sodre & Cuevas \(1997\)](#); [Bailer-Jones et al. \(1998\)](#); [Warren et al. \(2005\)](#); [Re Fiorentin et al. \(2007\)](#); [Steiner et al. \(2009\)](#). The main idea behind the PCA technique through deterministic algorithm without hyperparameters is linear technique to reduce the dimensionality of data that is highly correlated by transforming the original set of vectors to a new set known as Principal Components to preserve the global structure of the data. In the manuscript, the first two most important Principal Components (PCA dimension 1 and PCA dimension 2) are held by rotating the vectors for preserving variance. Meanwhile, the more recent powerful t-SNE technique involving hyperparameters is a non-linear technique through non-deterministic or randomised algorithm. The math behind t-SNE is quite complex but the idea is simple. It embeds the points from a higher dimension to a lower dimension trying to preserve the neighborhood of that point, preserving the local structure (cluster) of data. More specifically, t-SNE technique minimizes the divergence between two distributions: a distribution that measures pairwise similarities of the high-dimensional data and a distribution that measures pairwise similarities of the corresponding low-dimensional points in the embedding. In the manuscript,

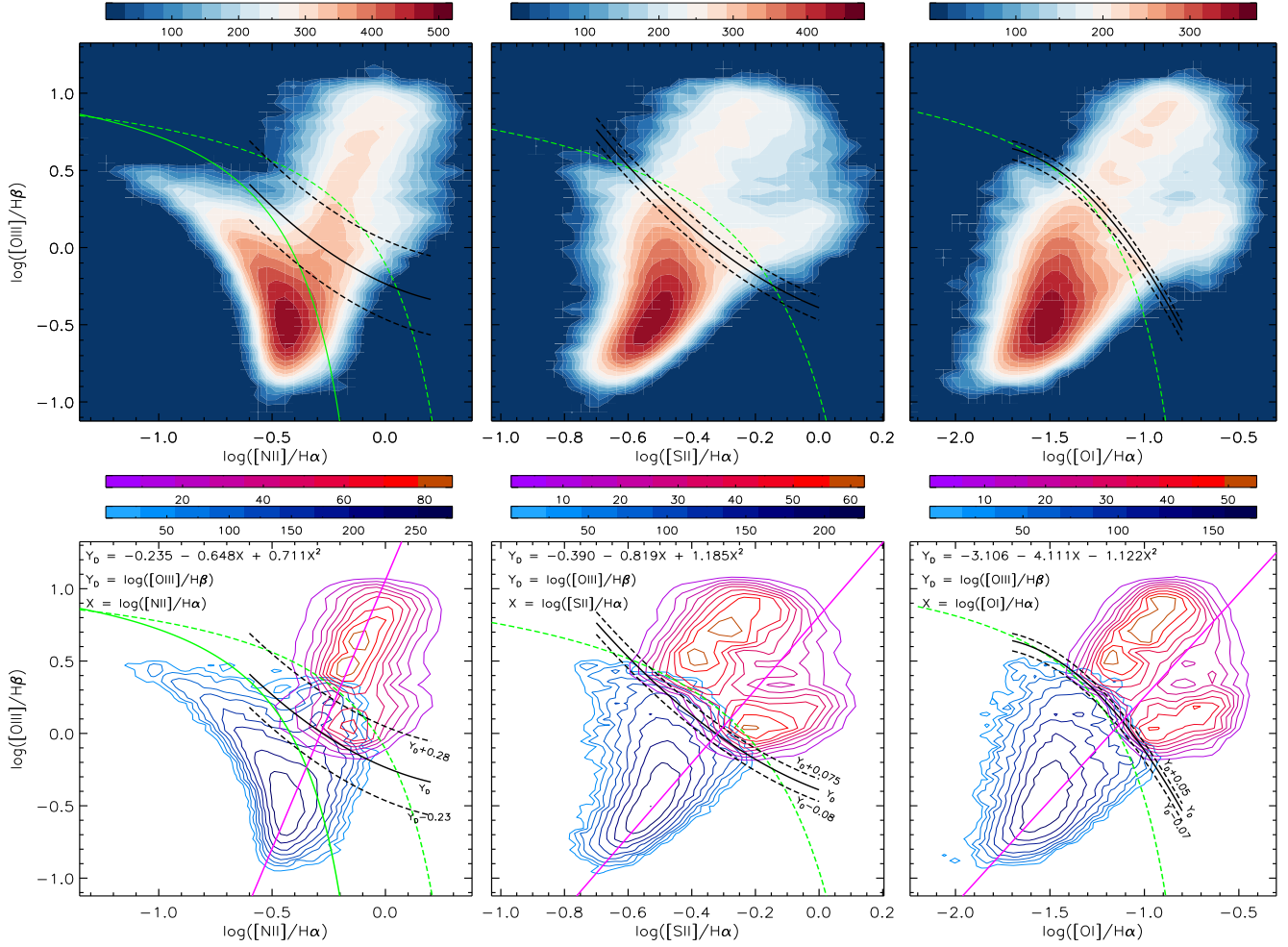


Figure 1. Properties of local narrow emission-line galaxies and dividing lines in BPT diagrams. **top panels** show the well-known three BPT diagrams in contour maps by flux ratios of $[\text{OIII}]/\text{H}\beta$, $[\text{NII}]/\text{H}\alpha$, $[\text{SII}]/\text{H}\alpha$ and $[\text{OI}]/\text{H}\alpha$ for the collected 35857 local narrow emission-line galaxies in SDSS DR15. Color bars show the corresponding number densities for the contour levels. **Bottom panels** show the corresponding two contour maps in the three BPT diagrams for the objects in the two clusters shown in Figure 2 determined by the t-SNE technique: the contour with contour lines near to red colors represents the map for the 7169 objects shown in red dots in Figure 2, the contour with contour lines near to blue colors represents the map for the 28688 objects shown in blue dots in Figure 2. Color bars with colors near to blue and near to red show the corresponding number densities for the levels in the two contours, respectively. In each bottom panel, solid line in magenta shows the referenced direction, in order to create series of strips to determine the crossover data points of the position dependent number ratios of the objects in the two clusters shown in Figure 2 included in the strips. In each panel, dashed line in green shows the photoionization model determined dividing line between extremely starburst galaxies and type-2 AGN (or the extreme outer boundary for HII galaxies) reported in Kewley et al (2001, 2006). Solid lines in green in the left panels show the dividing line between HII galaxies and composite galaxies reported in Kauffmann et al. (2003). In each panel, solid line in black shows the t-SNE technique determined dividing line Y_D , the expected dividing lines between type-2 AGN and HII galaxies, and dashed lines in black show the corresponding upper and lower boundaries of Y_{upper} and Y_{lower} .

the determined similarity of data points are shown in the corresponding reduced two-dimensional embedded space, i.e., the t-SNE dimension 1 and t-SNE dimension 2. Moreover, the commonly accepted hyperparameters applied in the t-SNE technique are perplexity, early exaggeration, learning rate and number of steps (the hyperparameters listed in sklearn.manifold.TSNE in python). Not similar as PCA technique, the t-SNE technique cannot preserve variance (global structure) but preserve distance using hyperparameters (local structure). Therefore, the non-linear and probabilistic t-SNE technique can often find fine structures where the PCA technique cannot.

Considering the four-dimensional data including the line ratios of $[\text{O III}]\lambda 5007\text{\AA}$ to narrow $\text{H}\beta$ ($[\text{OIII}]/\text{H}\beta$), $[\text{N II}]\lambda 6583\text{\AA}$ to narrow $\text{H}\alpha$ ($[\text{NII}]/\text{H}\alpha$), total $[\text{S II}]$ to narrow $\text{H}\alpha$ ($[\text{SII}]/\text{H}\alpha$) and $[\text{O I}]\lambda 6300\text{\AA}$ to narrow $\text{H}\alpha$ ($[\text{OI}]/\text{H}\alpha$) of the 35857 local narrow emission-line objects, the four line ratios applied in the three BPT diagrams, the data reduction and visualization can be well

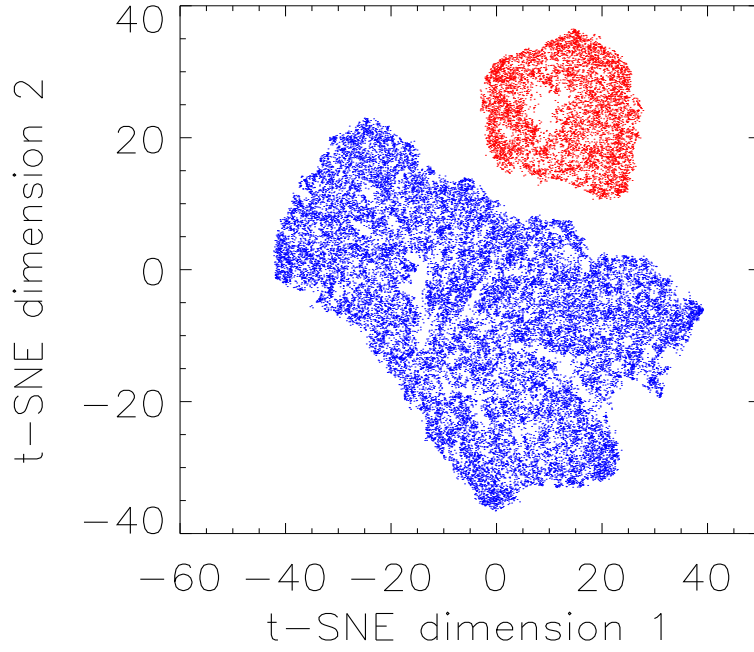


Figure 2. The t-SNE technique determined 2D projection of the collected 35857 local narrow emission-line galaxies through properties of the four narrow line ratios of $[\text{OIII}]/\text{H}\beta$, $[\text{NII}]/\text{H}\alpha$, $[\text{SII}]/\text{H}\alpha$ and $[\text{OI}]/\text{H}\alpha$ applied in the BPT diagrams. There are two clusters: one cluster with dots in red and the other cluster with dots in blue.

done through the two mathematical techniques. Figure 2 shows the two-dimensional projected map through the t-SNE technique applied to the four-dimensional data of the 35857 narrow emission-line objects. Here, the accepted hyperparameters applied in the t-SNE technique are [170, 5, 400, 800] for perplexity, early exaggeration, learning rate and number of steps, respectively. As we know that the powerful t-SNE technique is a particularly better technique than the PCA technique to especially do visualization of high-dimensional datasets, the t-SNE technique can clearly lead to nice two clusters shown in blue dots for 28688 objects and in red dots for 7169 objects in Figure 2. Meanwhile, the PCA technique cannot lead to similar results, compared results from the PCA technique and from the t-SNE technique are shown in the following Figure 4 and Figure 5.

The nice two clusters well determined by the t-SNE technique can strongly indicate intrinsic different physical properties in the BPT diagrams for the objects in the two clusters shown in Figure 2. Then, the narrow emission-line objects in the two clusters determined by the t-SNE technique are separately replotted in the BPT diagrams in bottom panels of Figure 1 with contour lines in bluish colors (for the objects shown in blue dots in Figure 2) and in reddish colors (for the objects shown in red dots in Figure 2), respectively. Then, based on the contours with contour lines in different colors in the BPT diagrams, it is interesting that the narrow emission-line objects in the two clusters shown in Figure 2 can be well distinguished in the BPT diagrams in bottom panels of Figure 1, providing the chance to determine dividing lines between HII galaxies and type-2 AGN by independent mathematical methods.

In the BPT diagram of $[\text{OIII}]/\text{H}\beta$ versus $[\text{NII}]/\text{H}\alpha$, there are two well accepted dividing lines between HII galaxies, composite galaxies and type-2 AGN, one is applied to determine the outer boundary for extremely starburst galaxies, and the other one is applied to determine the pure HII galaxies without central AGN activities, the region between the two dividing lines are well defined for composite galaxies. Now, in the bottom-left panel of Figure 1, the two previously defined dividing lines can be roughly compared with properties of the objects in the two clusters, considering the far-side outer boundaries for the objects in the two clusters. Meanwhile, the theoretical model determined dividing lines in the other two BPT diagrams can also be well compared with almost overlapped far-side boundaries of the objects in the two clusters determined by the t-SNE technique.

In order to construct a definite dividing line in the BPT diagram of $[\text{OIII}]/\text{H}\beta$ versus $[\text{NII}]/\text{H}\alpha$ between the objects in the two clusters determined by the t-SNE technique, a simple method has been applied. Followed a series of parallel strips with directions parallel to the referenced direction linked the ridges of the two contour maps of the objects in the two clusters, the dividing line

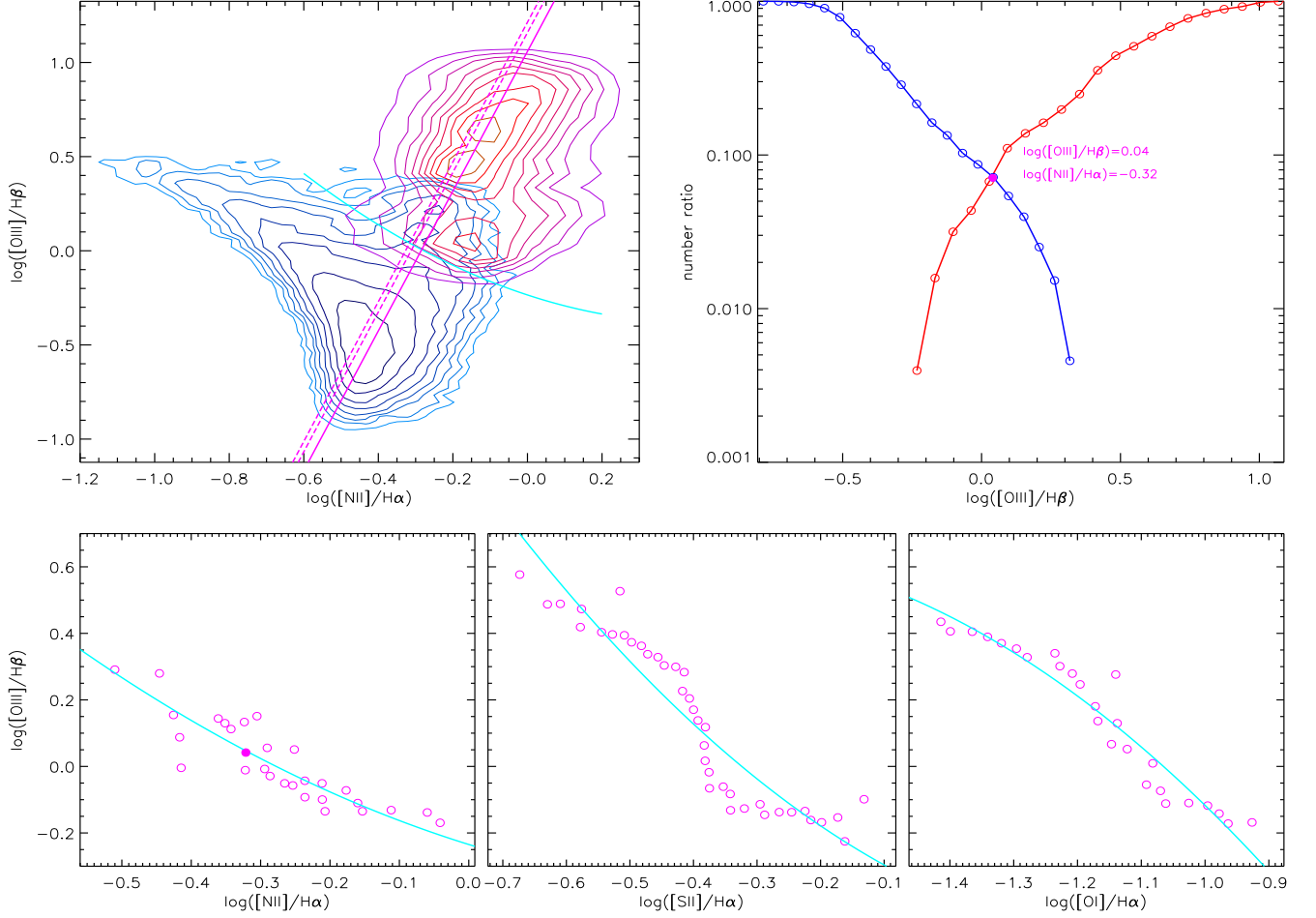


Figure 3. Detailed example on determining dividing lines in BPT diagrams. **Top-left panel** shows an example of the strip marked by two dashed lines in magenta with directions parallel to the given referenced direction shown in the solid line in magenta (same as the one shown in bottom-left panel of Figure 1). Solid line in cyan shows the determined dividing line. The two contours represent the maps for the objects in the two clusters shown in Figure 2. **Top-right panel** shows the normalized cumulative position-dependent number ratios of the objects included in the strip shown in the top-left panel from the objects in the two clusters with contour maps shown in colors near to blue and in colors near to red. Solid circle in magenta in the panel shows the crossover point of the two position dependent number ratios of the objects from the two clusters in the strip shown in the top-left panel. The position information of the crossover point is marked with characters in magenta. **Bottom panels** show the determined crossover points shown as open circles in magenta from a series of strips in the three BPT diagrams, and the 2-degree polynomial functions shown as solid lines in cyan applied to describe the data points. Solid circle in magenta in the bottom-left panel shows the crossover point determined in the top-right panel by the objects in the strip shown in the top-left panel.

Y_D is well built by the crossover points of the position dependent number ratios for the objects in the two clusters in the strips. The final dividing line Y_D has been well determined and shown in bottom-left panel of Figure 1. In the other two BPT diagrams, the referenced directions are given by the direction linked the ridge of the contour map in bluish colors and the gully of the other contour map in reddish colors, then leading to the t-SNE technique determined dividing lines Y_D . Moreover, totally similar results can be determined and confirmed in the BPT diagrams by given slightly different referenced directions but followed from the bottom-left to the top-right in the BPT diagrams. Here, Figure 3 shows an example on more detailed information on the crossover points for the objects in the two clusters in strips in the BPT diagrams.

Meanwhile, besides the t-SNE technique determined dividing lines Y_D described by the two-degree polynomial functions shown in Figure 1 and Figure 3, it will be very interesting to discuss properties of overlapped regions covered by both HII galaxies and type-2 AGN in the BPT diagrams. It is clear that when the objects in the two clusters are plotted in the BPT diagrams with their measured flux ratios of narrow emission lines (such as the results shown in bottom panels of Figure 1), there are overlapped regions in the BPT diagrams for the objects in the two clusters determined by the t-SNE technique. Therefore, the overlapped

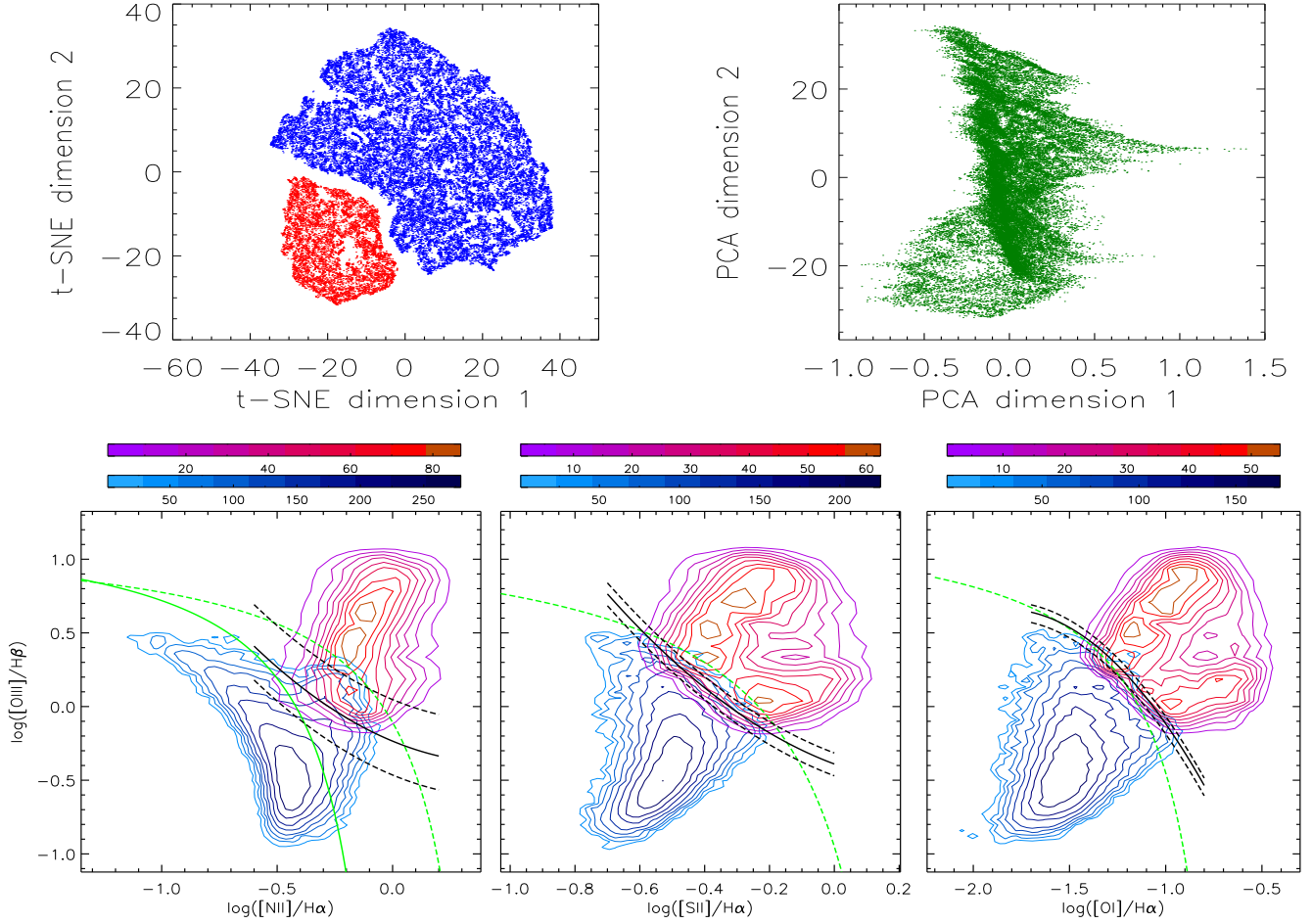


Figure 4. Properties of narrow emission-line galaxies and dividing lines in BPT diagrams by t-SNE technique with different hyper-parameters. **Top panels** show the 2D projections of the four-dimensional data of narrow emission line ratios of the 35857 narrow emission-line galaxies through the t-SNE technique (top-left panel) with hyper-parameters different from the ones applied in Figure 2 and through the PCA technique (top-right panel). **Bottom panels** show the corresponding two contour maps in the three well-known BPT diagrams for the objects in the two clusters determined by the t-SNE technique: the contour with contour lines near to red colors represents the map for the objects shown in red dots in the top-left panel, and the contour with contour lines near to blue colors represents the map for the objects shown in blue dots in the top-left panel. Color bars in different colors show the corresponding number densities for the contour levels. In bottom panels, dashed lines in green show the photoionization model determined dividing lines between extremely starburst galaxies and type-2 AGN reported in Kewley et al. (2001, 2006). Solid line in green in the bottom-left panel shows the dividing line between HII galaxies and composite galaxies reported in Kauffmann et al. (2003). Solid and dashed lines in black in each bottom panel show the dividing line Y_D and the corresponding upper and lower boundaries of Y_{upper} and Y_{lower} , the ones shown in Figure 1.

regions in the BPT diagrams are very real, which will provide further clues on properties of composite galaxies. Then, a simple mathematical idea is accepted to determine the overlapped regions between $Y_{upper} = Y_D + U$ and $Y_{lower} = Y_D - B$. Here, parameters of U and B are determined by the criteria that 1% of HII galaxies are above Y_{upper} and 1% of type-2 AGN are below Y_{lower} in the BPT diagrams of $[NII]/H\alpha$ versus $[OIII]/H\beta$ and $[SII]/H\alpha$ versus $[OIII]/H\beta$, but 0.5% of HII galaxies are above Y_{upper} and 0.5% of type-2 AGN are below Y_{lower} in the BPT diagram of $[OI]/H\alpha$ versus $[OIII]/H\beta$ (mainly due to the following shown very smaller overlapped region). The well determined boundaries Y_{upper} and Y_{lower} are shown in Figure 1.

For the results shown in bottom-left panel of Figure 1, the overlapped region is determined between $Y_{upper} = Y_D + 0.28$ and $Y_{lower} = Y_D - 0.23$ in the BPT diagram of $[NII]/H\alpha$ versus $[OIII]/H\beta$, meaning that 99% of HII galaxies are locating below the upper boundary of Y_{upper} and 99% of type-2 AGN are locating above the lower boundary of Y_{lower} . Therefore, we can simply say that the overlapped regions defined by the upper and lower boundaries of Y_{upper} and Y_{lower} represent the mixed region of HII galaxies and type-2 AGN with significant confidence level of 99%. Furthermore, the region between Y_{upper} and

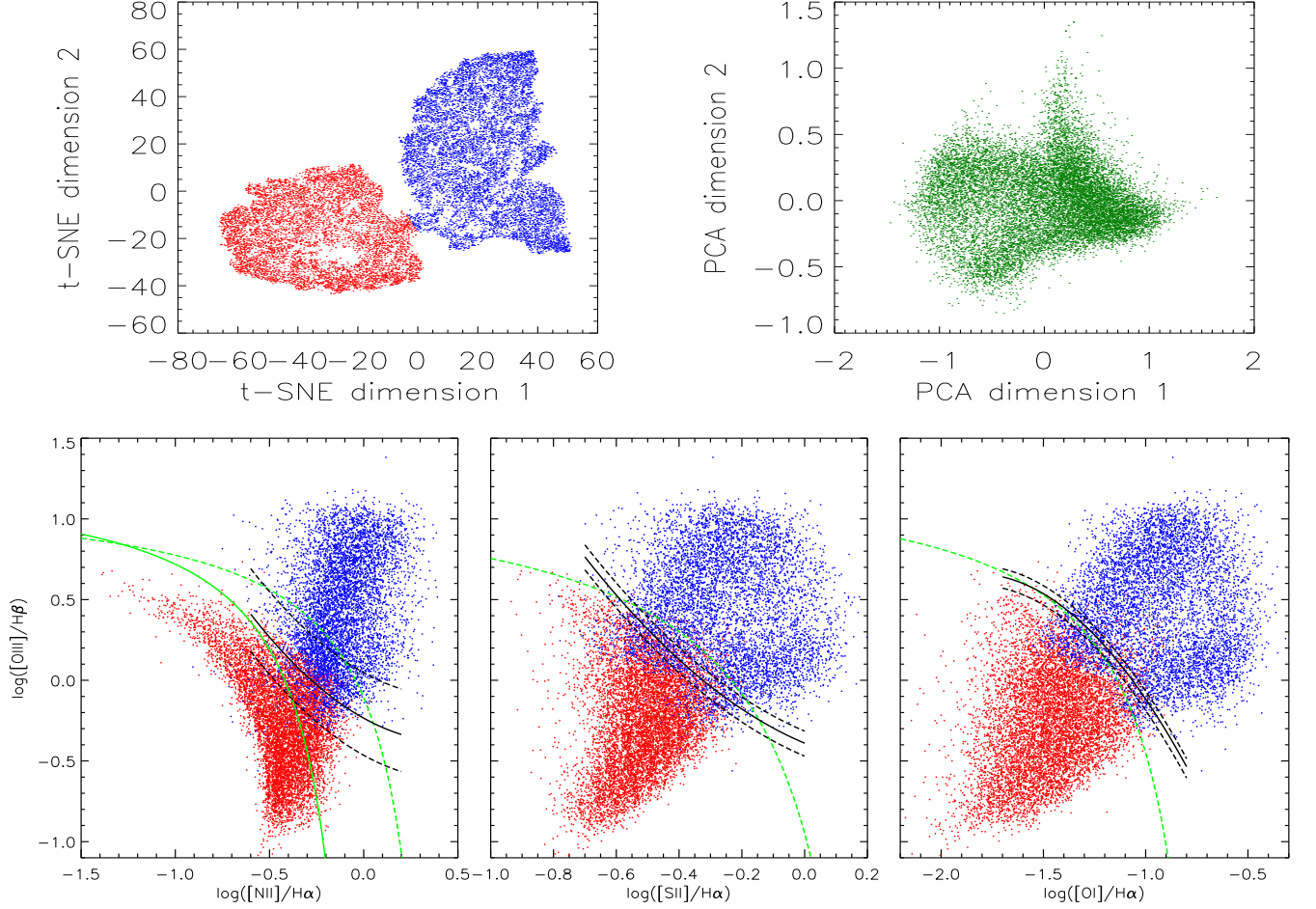


Figure 5. Properties of narrow emission-line galaxies and dividing lines in BPT diagrams by the t-SNE technique applied to the smoothed sample of narrow emission-line galaxies. **Top panels** show the 2D projections of the four-dimensional data of narrow emission line ratios of the smoothed 14554 narrow emission-line galaxies through the t-SNE technique (top-left panel) and through the PCA technique (top-right panel). **Bottom panels** show the three BPT diagrams for the 14554 galaxies in the two clusters determined by the t-SNE technique: small pluses in red and blue represent the objects shown in red dots and in blue dots in the top-left panel. In bottom panels, dashed lines in green show the photoionization model determined dividing lines between extremely starburst galaxies and type-2 AGN reported in Kewley et al. (2001, 2006). Solid line in green in the bottom-left panel shows the dividing line between HII galaxies and composite galaxies reported in Kauffmann et al. (2003). Solid and dashed lines in black in each bottom panel show the dividing line Y_D and the corresponding upper and lower boundaries of Y_{upper} and Y_{lower} , the ones shown in Figure 1.

Y_{lower} has interestingly similar covered space as the region between the reported dividing lines in Kewley et al. (2001, 2006) and in Kauffmann et al. (2003). However, there are no reports on composite galaxies in the BPT diagrams of $[SII]/H\alpha$ versus $[OIII]/H\beta$ and $[OI]/H\alpha$ versus $[OIII]/H\beta$ in the literature. We directly accepted the same criterion applied in the BPT diagram of $[NII]/H\alpha$ versus $[OIII]/H\beta$. Then, the upper and lower boundaries of $Y_{upper} = Y_D + 0.075$ and $Y_{lower} = Y_D - 0.08$ have been determined and shown in the bottom-middle panel of Figure 1 in the BPT diagram of $[SII]/H\alpha$ versus $[OIII]/H\beta$. Meanwhile, the overlapped region by the same criterion in the BPT diagram of $[OI]/H\alpha$ versus $[OIII]/H\beta$ is too small to be shown. Thereby, a smaller percentage of 0.5% than 1% is applied to determine the upper and lower boundaries of $Y_{upper} = Y_D + 0.05$ and $Y_{lower} = Y_D - 0.07$ shown in the BPT diagram of $[OI]/H\alpha$ versus $[OIII]/H\beta$ in the bottom-right panel of Figure 1.

It is very interesting that there is a larger overlapped area between Y_{upper} and Y_{lower} for composite galaxies in the BPT diagram of $[NII]/H\alpha$ versus $[OIII]/H\beta$, but much smaller overlapped areas in the BPT diagrams of $[OI]/H\alpha$ versus $[OIII]/H\beta$ and $[SII]/H\alpha$ versus $[OIII]/H\beta$. Therefore, the BPT diagram of $[NII]/H\alpha$ versus $[OIII]/H\beta$ is more efficient and powerful to classify the composite galaxies than the other two BPT diagrams. And moreover, the defined composite galaxies in the BPT diagram of $[NII]/H\alpha$ versus $[OIII]/H\beta$ cannot be totally in the right places for composite galaxies in the other two BPT diagrams of $[OI]/H\alpha$

versus $[\text{OIII}]/\text{H}\beta$ and $[\text{SII}]/\text{H}\alpha$ versus $[\text{OIII}]/\text{H}\beta$. The different properties of composite galaxies in different BPT diagrams reflect interesting but different dependence of forbidden emission lines on intrinsic different kinds of activities from AGN or from star-forming.

Finally, more detailed discussions have been shown on robust results through the t-SNE technique by the following two ways. On the one hand, besides the results shown in Figure 1 and Figure 2, Figure 4 shows similar results confirmed through the t-SNE technique applied with different hyper-parameters to the same four-dimensional data of narrow line ratios of the collected 35857 narrow emission-line galaxies. Here, the accepted hyperparameters re-applied in the t-SNE technique are [50, 10, 80, 1000] for perplexity, early exaggeration, learning rate and number of steps, respectively. Two definite data clusters can be re-confirmed and similar final results can be re-confirmed in the BPT diagrams as the results shown in Figure 1. On the other hand, in order to reduce computational complexity, especially to reduce probable effects of much different number densities of the objects in different regions of BPT diagrams, the BPT diagrams have been well smoothed leading to the almost even number densities in different regions with total 14554 objects collected from the 35857 objects, which are shown in bottom panels of Figure 5. Then, the similar t-SNE and PCA techniques are applied to do the data reduction and visualization of the four-dimensional data of the smoothed 14554 narrow emission-line galaxies. Here, the accepted hyperparameters applied in the t-SNE technique are [150, 5, 100, 800] for perplexity, early exaggeration, learning rate and number of steps, respectively. Top panels of Figure 5 show the 2D projections by the t-SNE and PCA techniques. Nice two clusters can be well confirmed by the t-SNE technique. Bottom panels of Figure 5 show properties of the objects in the two clusters and then the dividing lines applied in the BPT diagrams for the 14554 narrow emission-line galaxies.

Before the end of the section, there is one point we should note. As what we have known, there are two subsamples included in type-2 AGN: Seyfert galaxies and LINERs, and moreover, there are reported dividing lines between LINERs and Seyfert galaxies in the BPT diagrams, such as the results shown in Kewley et al. (2006) and in Schawinski et al. (2007). However, as the discussed results in de Souza et al. (2017), the Gaussian mixture model can not provide statistical evidence for the existence of a Seyfert/LINER dichotomy for the emission-line galaxies from SDSS DR7. Moreover, as the shown results through the t-SNE technique in Figure 2, in top-left panel of Figure 4 and in top-left panel of Figure 5, we cannot yet find a third data cluster determined by the t-SNE technique. More efforts should be necessary on constructing a new high-dimensional data including more valuable information. Therefore, at the current stage, we can not provide clear clues on the dividing lines between LINERs and Seyfert galaxies through the t-SNE technique, and we do not show further discussions any more on dividing lines between LINERs and Seyfert galaxies in the manuscript.

3. CONCLUSIONS

BPT diagrams are powerful tools for classifying narrow emission-line galaxies with different central activity properties. However, how to define the dividing lines in the BPT diagrams between different kinds of narrow emission-line galaxies is always an interesting challenge. Here, we can find well defined dividing lines through the pure mathematical t-SNE technique applied to the local narrow emission-line galaxies in SDSS DR15. The results not only show the charming harmonization of the theoretical expectations and the actual results from real observed properties through the powerful t-SNE technique, and also provide further confirmation on classification of the composite galaxies more efficiently in the BPT diagram of $[\text{OIII}]/\text{H}\beta$ versus $[\text{NII}]/\text{H}\alpha$.

ACKNOWLEDGEMENTS

Zhang, Feng, Chen and Yuan gratefully acknowledge the anonymous referee for giving us constructive comments and suggestions to greatly improve our paper. Zhang gratefully thanks the grant support from Nanjing Normal University and the grant support from NSFC-11973029. Yuan gratefully thanks the grant support from NSFC-11873032. This paper has made use of the data from the SDSS projects. The SDSS-III web site is <http://www.sdss3.org/>. SDSS-III is managed by the Astrophysical Research Consortium for the Participating Institutions of the SDSS-III Collaboration.

REFERENCES

- | | |
|---|--|
| <p>Aguado, D. S.; Ahumada, R.; Almeida, A.; et al., 2019, ApJS, 240, 23</p> <p>Anders, F.; Chiappini, C.; Santiago, B. X.; et al., 2018, A&A, 619, 125</p> <p>Arora S.; Hu W.; Kothari P. K., 2018, Proceedings of Machine Learning Research, 75, 1</p> | <p>Bailer-Jones, C. A. L.; Irwin, M.; von Hippel, T., 1998, MNRAS, 298, 361</p> <p>Baldwin, J. A.; Phillips, M. M.; Terlevich, R., 1981, PASP, 93, 5</p> <p>Belfiore, F.; Westfall, K. B.; Schaefer, A.; et al., 2019, AJ, 158, 160</p> <p>Binette, L.; Magris, C. G.; Stasińska, G.; Bruzual, A. G., 1994, A&A, 292, 13</p> |
|---|--|

- Cid Fernandes, R.; Stasinska, G.; Mateus, A.; et al., 2011, MNRAS, 413, 1687
- de Souza, R. S.; Dantas, M. L. L.; Costa-Duarte, M. V.; et al. 2017, MNRAS, 472, 280**
- Dopita, M. A. & Sutherland, R. S., 1995, ApJ, 455, 468
- Dopita, M. A. & Sutherland, R. S., 1996, ApJS, 102, 161
- Eracleous, M.; Hwang, J. A.; Flohic, H. M. L. G., 2010, ApJ, 711, 796
- Ferland, G. J.; Netzer, H., 1983, ApJ, 264, 105
- Filippenko, A. V. & Terlevich, R., 1992, ApJL, 397, 79
- Groves, B. A.; Dopita, M. A.; Sutherland, R. S., 2004, ApJS, 153, 75
- Halpern, J. P.; Steiner, J. E., 1983, ApJL, 269, 37
- Heckman, T. M., 1980, A&A, 87, 152
- Ian Jolliffe, T.; Cadima, J., 2016, Phil. Trans. R. Soc. A., 374, 20150202
- Juneau, S.; Bournaud, F.; Charlot, S.; et al., 2014, ApJ, 788, 88
- Kauffmann, G.; Heckman, T. M.; Tremonti, C.; et al., 2003, MNRAS, 346, 1055
- Kashino, D.; Silverman, J. D.; Sanders, D.; et al., 2017, ApJ, 835, 88
- Kewley, L. J.; Dopita, M. A.; Sutherland, R. S.; Heisler, C. A.; Trevena, J., 2001, ApJ, 556, 121
- Kewley, L. J.; Nicholls, D. C.; Sutherland, R. S., 2019, ARA&A, 57, 511
- Kewley, L. J.; Groves, B.; Kauffmann, G.; et al., 2006, MNRAS, 372, 961
- Lever, J.; Krzywinski, M.; Altman, N., 2017, Nature Method, 16, 641
- Levesque, E. M.; Kewley, L. J.; Larson, K. L., 2010, AJ, 139, 712
- Marquez I., Masegosa J., Gonzalez-Martin O., et al., 2017, Frontiers in Astronomy and Space Sciences, 4, 34
- Melendez, M.; Heckman, T. M.; Martinez-Paredes, M.; Kraemer, S. B.; Mendoza, C., 2014, MNRAS, 443, 1358
- Re Fiorentin, P.; Bailer-Jones, C. A. L.; Lee, Y. S., et al., 2007, A&A, 467, 1373
- Schawinski, K.; Thomas, D.; Sarzi, M.; et al., 2007, MNRAS, 382, 1415
- Sodre, L.; Cuevas, H., 1997, MNRAS, 287, 137
- Stasinska, G.; Cid Fernandes, R.; Mateus, A.; et al., 2006, MNRAS, 371, 972
- Steiner, J. E.; Menezes, R. B.; Ricci, T. V.; Oliveira, A. S., 2009, MNRAS, 395, 64
- Steinhardt, C. L.; Weaver, J. R.; Maxfield, J.; et al., 2020, ApJ, 891, 136
- Terlevich, R.; Melnick, J., 1985, MNRAS, 213, 841
- Traven, G.; Matijevic, G.; Zwitter, T.; et al., 2017, ApJS, 228, 24
- van der Maaten, L.; Hinton, G., 2008, Journal of Machine Learning Research, 9, 2579
- van der Maaten, L., 2014, Journal of Machine Learning Research, 15, 3221
- Veilleux, S. & Osterbrock, D. E., 1987, ApJS, 63, 295
- Warren, J. S.; Hughes, J. P.; Badenes, C.; et al., 2005, ApJ, 634, 376